

# A repeating fast radio burst source in a globular cluster

F. KIRSTEN,<sup>1</sup> B. MARCOTE,<sup>2</sup> K. NIMMO,<sup>3,4</sup> J. W. T. HESSELS,<sup>4,3</sup> M. BHARDWAI,<sup>5,6</sup> S. P. TENDULKAR,<sup>7,8</sup> A. KEIMPEMA,<sup>2</sup> J. YANG,<sup>1</sup> M. P. SNELDERS,<sup>4</sup> P. SCHOLZ,<sup>9</sup> A. B. PEARLMAN,<sup>5,6,10,11,12</sup> C. J. LAW,<sup>13,14</sup> W. M. PETERS,<sup>15</sup> M. GIROLETTI,<sup>16</sup> D. M. HEWITT,<sup>4</sup> U. BACH,<sup>17</sup> V. BEZUKOV,<sup>18</sup> M. BURGAY,<sup>19</sup> S. T. BUTTACCO,<sup>20</sup> J. E. CONWAY,<sup>1</sup> A. CORONGIU,<sup>19</sup> R. FEILER,<sup>21</sup> O. FORSSÉN,<sup>1</sup> M. P. GAWROŃSKI,<sup>21</sup> R. KARUPPUSAMY,<sup>17</sup> M. A. KHARINOV,<sup>22</sup> M. LINDQVIST,<sup>1</sup> G. MACCAFERRI,<sup>16</sup> A. MELNIKOV,<sup>22</sup> O. S. OULD-BOUKATTINE,<sup>4</sup> Z. PARAGI,<sup>2</sup> A. POSSENTI,<sup>19,23</sup> G. SURCIS,<sup>19</sup> N. WANG,<sup>24</sup> J. YUAN,<sup>24</sup> K. AGGARWAL,<sup>25,26</sup> R. ANNA-THOMAS,<sup>25,26</sup> G. C. BOWER,<sup>27</sup> R. BLAAUW,<sup>3</sup> S. BURKE-SPOLAOR,<sup>25,26,28</sup> T. CASSANELLI,<sup>9,29</sup> T. E. CLARKE,<sup>15</sup> E. FONSECA,<sup>5,6,25,26</sup> B. M. GAENSLER,<sup>9,29</sup> A. GOPINATH,<sup>4</sup> V. M. KASPI,<sup>5,6</sup> N. KASSIM,<sup>15</sup> T. J. W. LAZIO,<sup>30</sup> C. LEUNG,<sup>31,32</sup> D. LI,<sup>13</sup> H. H. LIN,<sup>33</sup> K. W. MASUI,<sup>31,32</sup> R. MCKINVEN,<sup>9</sup> D. MICHILLI,<sup>5,6</sup> A. MIKHAILOV,<sup>22</sup> C. NG,<sup>9</sup> A. ORBIDANS,<sup>18</sup> U. L. PEN,<sup>33,9,28,34</sup> E. PETROFF,<sup>4,5,6,35</sup> M. RAHMAN,<sup>36</sup> S. M. RANSOM,<sup>37</sup> K. SHIN,<sup>31,32</sup> K. M. SMITH,<sup>34</sup> I. H. STAIRS,<sup>38</sup> AND W. VLEMINGS<sup>1</sup>

<sup>1</sup>Department of Space, Earth and Environment, Chalmers University of Technology, Onsala Space Observatory, 439 92, Onsala, Sweden

<sup>2</sup>Joint Institute for VLBI ERIC, Oude Hoogeveensedijk 4, 7991 PD Dwingeloo, The Netherlands

<sup>3</sup>ASTRON, Netherlands Institute for Radio Astronomy, Oude Hoogeveensedijk 4, 7991 PD Dwingeloo, The Netherlands

<sup>4</sup>Anton Pannekoek Institute for Astronomy, University of Amsterdam, Science Park 904, 1098 XH, Amsterdam, The Netherlands

<sup>5</sup>Department of Physics, McGill University, 3600 rue University, Montréal, QC H3A 2T8, Canada

<sup>6</sup>McGill Space Institute, McGill University, 3550 rue University, Montréal, QC H3A 2A7, Canada

<sup>7</sup>Department of Astronomy and Astrophysics, Tata Institute of Fundamental Research, Mumbai, 400005, India

<sup>8</sup>National Centre for Radio Astrophysics, Post Bag 3, Ganeshkhind, Pune, 411007, India

<sup>9</sup>Dunlap Institute for Astronomy & Astrophysics, University of Toronto, 50 St. George Street, Toronto, ON M5S 3H4, Canada

<sup>10</sup>Division of Physics, Mathematics, and Astronomy, California Institute of Technology, Pasadena, CA 91125, USA

<sup>11</sup>McGill Space Institute (MSI) Fellow

<sup>12</sup>FRQNT Postdoctoral Fellow

<sup>13</sup>Cahill Center for Astronomy and Astrophysics, California Institute of Technology, 1216 E California Boulevard, Pasadena, CA 91125, USA

<sup>14</sup>Owens Valley Radio Observatory, California Institute of Technology, Pasadena, CA 91125, USA

<sup>15</sup>Remote Sensing Division, US Naval Research Laboratory, Washington, DC 20375, USA

<sup>16</sup>Istituto Nazionale di Astrofisica, Istituto di Radioastronomia, via Gobetti 101, I-40129 Bologna, Italy

<sup>17</sup>Max Planck Institute for Radio Astronomy, Auf dem Heugel 69 53121 Bonn, Germany

<sup>18</sup>Engineering Research Institute Ventspils International Radio Astronomy Centre (ERI VIRAC) of Ventspils University of Applied Sciences (VUAS), Inzenieru street 101, Ventspils, LV-3601, Latvia

<sup>19</sup>Istituto Nazionale di Astrofisica, Osservatorio Astronomico di Cagliari, Via della Scienza 5, I-09047, Selargius, Italy

<sup>20</sup>Istituto Nazionale di Astrofisica, Istituto di Radioastronomia Radiotelescopio di Noto, C.da Renna Bassa Loc. Case di Mezzo C.P. 161, 96017, Noto (SR), Italy

<sup>21</sup>Institute of Astronomy, Faculty of Physics, Astronomy and Informatics, Nicolaus Copernicus University, Grudziadzka 5, 87-100 Toruń, Poland

<sup>22</sup>Institute of Applied Astronomy of the Russian Academy of Sciences, Kutuzova Embankment 10, St. Petersburg, 191187, Russia

<sup>23</sup>Università di Cagliari, Dipartimento di Fisica, S.P. Monserrato-Sestu Km 0,700 - 09042 Monserrato (CA), Italy

<sup>24</sup>Xinjiang Astronomical Observatory, 150 Science 1-Street, Urumqi, Xinjiang 830011, China

<sup>25</sup>Department of Physics and Astronomy, West Virginia University, P.O. Box 6315, Morgantown, WV 26506, USA

<sup>26</sup>Center for Gravitational Waves and Cosmology, West Virginia University, Chestnut Ridge Research Building, Morgantown, WV 26505, USA

<sup>27</sup>Academia Sinica Institute of Astronomy and Astrophysics, 645 N. A'ohoku Place, Hilo, HI 96720, USA

<sup>28</sup>Canadian Institute for Advanced Research, CIFAR Azrieli Global Scholar, MaRS Centre West Tower, 661 University Ave. Suite 505, Toronto ON M5G 1M1, Canada

<sup>29</sup>David A. Dunlap Department of Astronomy & Astrophysics, University of Toronto, 50 St. George Street, Toronto, ON M5S 3H4, Canada

<sup>30</sup>Jet Propulsion Laboratory, California Institute of Technology, 4800 Oak Grove Dr, Pasadena, CA 91109, USA

<sup>31</sup>MIT Kavli Institute for Astrophysics and Space Research, Massachusetts Institute of Technology, 77 Massachusetts Ave, Cambridge, MA 02139, USA

<sup>32</sup>Department of Physics, Massachusetts Institute of Technology, 77 Massachusetts Ave, Cambridge, MA 02139, USA

<sup>33</sup>Canadian Institute for Theoretical Astrophysics, University of Toronto, 60 St. George Street, Toronto, ON, M5S 3H8, Canada

<sup>34</sup>Perimeter Institute for Theoretical Physics, 31 Caroline Street North, Waterloo, ON, N2L 2Y5, Canada

<sup>35</sup>Veni Fellow

<sup>36</sup>Sidrat Research, PO Box 73527 RPO Wychwood, Toronto, ON M6C 4A7, Canada

<sup>37</sup>National Radio Astronomy Observatory, 520 Edgemont Rd., Charlottesville, VA 22903, USA

<sup>38</sup>Dept. of Physics and Astronomy, University of British Columbia, 6224 Agricultural Road, Vancouver, BC V6T 1Z1

## ABSTRACT

Fast radio bursts (FRBs) are extremely luminous and brief radio flashes originating from other galaxies (Petroff et al. 2019). Progressing our understanding of the FRB phenomenon is limited by their large distances and unpredictable activity. The recent discovery of FRB 20200120E (Bhardwaj et al. 2021), in the direction of the M81 galaxy, offers the chance to study an exceptionally nearby repeating source. Here we conclusively prove that FRB 20200120E is associated with a globular cluster in the M81 galactic system, thereby confirming that it is 40 times closer than any other known extragalactic FRB (Marcote et al. 2020). Because such globular clusters host old stellar populations, this association challenges FRB models that invoke magnetars formed in a core-collapse supernova as powering FRB emission (e.g. CHIME/FRB Collaboration et al. 2020; Bochenek et al. 2020; Margalit & Metzger 2018; Murase et al. 2016). We propose that FRB 20200120E is a young, highly magnetised neutron star, formed via either accretion-induced collapse of a white dwarf or via merger of compact stars in a binary system. Alternative scenarios are giant pulses from millisecond pulsars and compact binary systems (Pooley et al. 2003), some either interacting through winds, magnetically, or actively accreting via a disc. Given the proximity of FRB 20200120E, our upper limits on associated persistent radio, X-ray and gamma-ray emission tightly constrain the possible source models.

*Keywords:* Fast Radio Bursts

## 1. INTRODUCTION

The large extragalactic distances to FRBs (luminosity distance  $d_L = 0.1\text{--}10 \text{ Gpc}$ ) present a formidable challenge in associating them with multi-wavelength counterparts (or even host galaxies, in the case of the most distant sources; e.g., Law et al. 2020). To date, the closest precisely localised repeater is FRB 20180916B, at  $d_L \sim 150 \text{ Mpc}$  (Marcote et al. 2020). At such a distance, joint radio and optical observations can probe transverse physical scales on the order of  $\sim 100 \text{ pc}$ . Thanks to the 2.3 milliarcsecond localisation precision provided by the European Very-long-baseline-interferometry Network (EVN), coupled with *Hubble Space Telescope* observations, it was possible to demonstrate that this source is near a region of active star formation in the host galaxy, but still significantly offset by  $\sim 250 \text{ pc}$  (Tendulkar et al. 2021). This suggests that the source of the bursts, presumably a neutron star, is not particularly young — or that the progenitor system had the time to move away from the nearby star-forming region before the neutron star was formed.

Compelling evidence for magnetar models of FRB emission came with the discovery of an extremely bright ( $\sim \text{MJy ms}$ ) FRB-like burst from the Galactic magnetar SGR 1935+2154 (CHIME/FRB Collaboration et al. 2020; Bochenek et al. 2020). This FRB-like event was accompanied by a prompt, hard X-ray burst (e.g., Mereghetti et al. 2020), and in the weeks thereafter additional, still relatively bright ( $\sim 100 \text{ Jy ms}$ ), radio bursts were detected (Kirsten et al. 2021). SGR 1935+2154 is associated with the supernova remnant SNR G57.2+0.8 at a distance of  $\sim 3\text{--}10 \text{ kpc}$  (e.g., Sieber & Seiradakis 1984; Kothes et al. 2018; Bailes et al. 2021; Zhou et al. 2020), and its proximity compared to the extragalactic FRBs greatly aids in its multi-wavelength

study. Because the MJy-ms burst from SGR 1935+2154 would still have been detectable at a distance of tens of Mpc, it has been argued that a notable fraction of FRBs are related to magnetar flares (CHIME/FRB Collaboration et al. 2020; Bochenek et al. 2020).

Recently, Bhardwaj et al. (2021) presented the discovery of the repeatedly bursting FRB 20200120E, made by CHIME/FRB. With a dispersion measure (DM) of only  $88 \text{ pc cm}^{-3}$ , this source must be relatively nearby ( $d_L < 135 \text{ Mpc}$ , Bhardwaj et al. 2021), and perhaps even in the halo of our own Milky Way galaxy. If FRB 20200120E is indeed extragalactic, then the DM excess compared to the Galactic contribution from the interstellar medium (ISM) and halo is only  $\sim 10\text{--}20 \text{ pc cm}^{-3}$ . This strongly constrains DM contributions from the Milky Way halo and local source environment. Importantly, FRB 20200120E lies in the direction of the grand design spiral galaxy M81 (also known as Bode’s Galaxy and NGC 3031; distance of 3.6 Mpc; Freedman et al. 1994), and more specifically towards the tidal bridge between M81 and the galaxy NGC 3077 (Yun 1999). M81 is the largest galaxy in a group of 34 (Karachentsev 2005), and represents one of the most massive nearby galaxies. As noted by Bhardwaj et al. (2021), if FRB 20200120E can be robustly associated with the M81 system, it would provide an unprecedented opportunity to study a remarkably nearby repeating FRB.

Here we present the sub-arcsecond localisation of FRB 20200120E using telescopes that are part of the EVN, and associate it with a globular cluster in the M81 galactic system. In §2 we present the new radio interferometric observations and archival optical, X-ray and gamma-ray observations used in this study. In §3 we present the results, and discuss their implications for our understanding of repeating FRBs in §4. In a companion paper, Nimmo

**Table 1.** Setups at the different stations

Telescope	Frequency coverage [MHz]	Station project code	EVN project code
Effelsberg (Ef)	1254 – 1510	94-20	EK048B, EK048C
Medicina (Mc)	1350 – 1478	44-20	EK048B, EK048C
Noto (Nt)	1318 – 1574	44-20	EK048C
Irbene (Ir)	1382 – 1510	–	EK048B, EK048C
Toruń (Tr)	1254 – 1510	DDT <sup>a</sup>	EK048B, EK048C
Westerbork (Wb)	1382 – 1510	DDT <sup>a</sup>	EK048B, EK048C
Urumqi (Ur)	1382 – 1510	DDT <sup>a</sup>	EK048C
VLA-VLITE	320 – 384	20B-280	–
<b>VLA-Realfast</b>	1300 – 1700	20B-280	–

<sup>a</sup>Director's Discretionary Time

et al. present a detailed, high-time resolution analysis of the spectro-polarimetric properties of the bursts used in this study.

## 2. OBSERVATIONS AND DATA REDUCTION

### 2.1. VLBI observations

As part of our ongoing very long baseline interferometry (VLBI) campaign called PRECISE (Pinpointing REpeating ChIMe Sources with the EVN), we observed the field centred on the coordinates  $\alpha$  (J2000) =  $09^{\text{h}}57^{\text{m}}56.688^{\text{s}}$ ,  $\delta$  (J2000) =  $68^{\circ}49'31.8''$  (Bhardwaj et al. 2021, who quote a 90% confidence interval of radius  $\sim 1.5'$ ) with an *ad-hoc* interferometric array composed of dishes that are part of the EVN. The data were taken on 2021 February 20 UT 17:00–22:00 (project code PR141A) and on 2021 March 7 UT 15:45–20:45 (PR143A). We observed in the 21-cm band ( $\sim 1.4$  GHz) with slightly different array setups in each run. Depending on the capabilities at each station, we recorded either 128 MHz or 256 MHz of total bandwidth, divided into 8 or 16 subbands of 16 MHz. The participating stations and their respective frequency coverage are summarised in Table 1. We ran regular phase-referencing observations with a cycle time of 7.5 min; i.e. 5.5 minutes on target and 2.0 minutes on the phase calibrator (J0955+6903, at  $\approx 0.32^\circ$  separation). In total, we spent 2.93 hrs on the target field in each observation. The calibrator source J1048+7143 served as fringe finder and bandpass calibrator and was observed twice for 5 minutes in each run. The pulsar B0355+54 was observed for verification and single-dish time-domain calibration purposes for another 2 minutes, once in each of the two observations.

We recorded raw voltages ('baseband' data, dual circular polarisation, 2-bit sampling) in VDIF (Whitney et al. 2010) format at all stations. At Effelsberg we also recorded total intensity filterbanks with the PSRIX pulsar backend (Lazarus et al. 2016) in parallel to the voltage data. These data span the frequency range of 1255–1505 MHz with a time and frequency resolution of 102.4  $\mu$ s and 0.49 MHz, respectively. The data from Effelsberg were searched for bursts in two in-

dependent pipelines. The voltage data were processed with the pipeline outlined in Kirsten et al. (2021), which converts the raw voltages to filterbank format (in this case, total intensity with time resolution 64  $\mu$ s and frequency resolution 125 kHz) and searches those with Heimdall within  $\pm 50$  pc cm $^{-3}$  of the expected DM = 87.818 pc cm $^{-3}$  as found by Bhardwaj et al. (2021). The burst candidates are classified as either radio frequency interference (RFI) or potential FRBs using the neural network classifier FETCH (Agarwal et al. 2020). The filterbanks as recorded with PSRIX were searched with a pipeline that uses the PRESTO suite of tools (Ransom 2001, 2011) and a classifier based on work by Michilli et al. (2018a).

Correlation of the data was performed at the Joint Institute for VLBI ERIC (JIVE; in the Netherlands) under proposal EK048 (with codes EK048B for PR141A and EK048C for PR143A). In total, we ran three correlator passes using the software correlator SFXC (Keimpema et al. 2015): in the first run we correlate all scans containing the calibrator sources with a standard 2-s time integration and 64 channels per 16-MHz subband. A second correlation pass was performed only on the data containing bursts (their arrival times were determined via the search described above), with a higher frequency resolution (8192 channels per subband) and time resolution (the correlation gates around the bursts were chosen manually to optimise the signal-to-noise for each burst, Table 2). The strongest bursts allowed a direct fringe fit on their data, which provided a first estimate of their sky position to a level of a few arcseconds:  $\alpha$  (J2000)  $\approx 09^{\text{h}}57^{\text{m}}54.8^{\text{s}}$ ,  $\delta$  (J2000)  $\approx 68^{\circ}49'03''$ . We then used this position to re-correlate the burst data at the same frequency resolution as in the first correlation pass. This allowed us to directly apply the calibration performed on the first pass (containing the calibrator sources) to the data containing bursts.

The full data reduction was performed using the Astronomical Image Processing System (AIPS, Greisen 2003) and DIFMAP (Shepherd et al. 1994) following standard pro-

cedures. *A-priori* amplitude calibration was performed using the known gain curves and system temperature measurements recorded at each station during the observation. These data were not available for Toruń and Irbene in EK048B, and for Urumqi in EK048C. We used nominal system equivalent flux density values and flat gain curves to perform the amplitude calibration in these cases. Ionospheric dispersive delays were calculated from maps of total electron content provided by the global positioning system satellites and removed via the TECOR task. We first corrected for the instrumental delays and bandpass calibration using the calibrator source J1048+7143, and thereafter fringe-fit the data using all calibrator sources. The phase calibrator (J0955+6903; displaying a peak brightness of  $\sim 73 \text{ mJy beam}^{-1}$ ) was then imaged and self-calibrated to improve the final calibration of the data (for both phases and amplitudes). A common source model for the phase calibrator was used to improve the calibration of both epochs. The obtained solutions were then transferred to the burst data, which were finally imaged.

In the third, and final, correlator pass we processed the entire observation, in order to obtain a deep continuum image of the field.

## 2.2. VLA

We observed the field of FRB 20200120E with the Karl G. Jansky Very Large Array (VLA) as part of a program to localise repeating FRBs identified by CHIME/FRB (program 20B-280). The field was observed in five 1-hour blocks from 2020 December 29 through 2021 January 18. Data were recorded in parallel at both 1.5 GHz and 340 MHz. The VLA antennas were arranged in the A configuration, which provides baseline lengths up to 30 km and a typical spatial resolution of  $1.3''$  and  $6.0''$  at 1.5 GHz and 340 MHz, respectively. The total on-target integration time amounts to 200 minutes.

### 2.2.1. *Realfast*

Visibility data from the VLA observations were recorded with a sampling time of 3 seconds from 1 to 2 GHz. Simultaneously, a copy of the data with sampling time of 10 ms was streamed into the *Realfast* system (Law et al. 2018). We used *Realfast* to search this data stream for FRBs in real time. The typical  $1\sigma$  sensitivity of the VLA is  $5 \text{ mJy beam}^{-1}$  in 10 ms.

The standard (slow) visibility data were analyzed to search for persistent emission associated with the FRB location. We calibrated the data with the VLA calibration pipeline (version 2020.1) using 3C147 as a flux calibrator. Calibrated visibilities for all five epochs were combined and imaged with CASA (version 6.1).

We imaged the data with robust weighting of 0.5 and removed baselines shorter than  $100\lambda$  to reduce the effects of RFI. This produced an image with a synthesized beam size of  $2''$  by  $1''$  with position angle of  $126^\circ$ . The sensitivity in

the combined image is  $6.5 \text{ }\mu\text{Jy beam}^{-1}$ , which is consistent with expectations given the usable bandwidth of 400 MHz.

### 2.2.2. VLITE

The VLA Low-band Ionosphere and Transient Experiment (VLITE; Polisensky et al. 2016; Clarke et al. 2016) is a commensal instrument on the VLA that records and correlates data from a 64-MHz subband at a central frequency of  $\sim 340$  MHz. It operates on up to 18 antennas during nearly all regular VLA operations. All VLITE data were processed within the VLITE-Fast GPU-based real-time system to search the incoming voltage stream for dispersed transients (Bethapudi et al. 2021). For imaging purposes, primary calibration and editing for each day of visibility data were carried out with the automated VLITE processing pipeline. Due to radio interference from satellites at the upper end of the band, the final usable bandwidth was 38.2 MHz centred at 340.85 MHz. The data were subsequently combined, imaged and self-calibrated in amplitude and phase using the Obit task MFIImage (Cotton 2008). In order to reduce artefacts from the bright extended radio galaxy M82 located  $\sim 1^\circ$  northwest of the target position, baselines shorter than  $4.0 \text{ k}\lambda$  were removed at this point. The final image was created in WS-Clean (Offringa et al. 2014), and corrected for the offset primary beam response of VLITE. The image has an rms of  $320 \text{ }\mu\text{Jy beam}^{-1}$ , and a beam of  $10.1''$  by  $3.6''$  at a position angle of  $132^\circ$ .

## 2.3. Archival optical and high energy data

### 2.3.1. Hyper Suprime-Cam

The field around M81 has been well-observed over the years by multiple telescopes. We retrieved archival data from the Hyper Suprime-Cam on the 8.1-m Subaru telescope (Miyazaki et al. 2012) using the SMOKA interface. We chose images with seeing better than  $0''.7$ . We processed the  $g'$ ,  $r'$ , and  $i'$  band images with the `hscpipev8.4` pipeline (Bosch et al. 2018). The pipeline uses the PanSTARRs catalogue (PS1; Flewelling et al. 2020) as an astrometric and photometric reference. The typical astrometric residuals were  $\sim 50$ – $60$  mas.

### 2.3.2. Chandra X-ray Observatory

Several deep archival X-ray observations are available for the field around M81 from *XMM* and *Chandra*. We selected the archival observation with the longest exposure time that covers the location of FRB 20200120E, a 26 ks *Chandra* observation (Obs. ID 9540, taken with ACIS in FAINT mode, Garmire et al. 2003) to probe for an X-ray source. The data were reduced using CIAO version 4.12 (Fruscione et al. 2006) following standard procedures. As the source was located about  $14'$  off-axis events were extracted in a large  $10''$ -radius region centred on the position of FRB 20200120E. We

also extract events from a 60''-radius region away from the source at a similar off-axis angle to estimate the background count rate.

### 2.3.3. *Fermi-LAT*

The Large Area Telescope (LAT) onboard *Fermi* provides a uniform sensitivity survey of the whole sky in the energy range between 100 MeV and 300 GeV. We searched all of the publicly available catalogues for counterparts up to the latest published release (4FGL-DR2, [Ballet et al. 2020](#)).

## 3. ANALYSIS & RESULTS

### 3.1. *Burst detection and localisation*

We found no bursts in the VLA *Realfast* or VLITE data. Blindly searching the EVN baseband data, we found two bursts (which we label B1 and B2, Figure 1) in the data taken on 2021 February 20, and another two bursts (B3 and B4, Figure 1) in the data taken on 2021 March 7. We found all bursts except B1 also in the data recorded with PSRIX, although the classifier initially flagged B2 as RFI because of its scintillation structure. The arrival time of B1 fell within the first few seconds of a recording and because of a delay between the start times of the baseband and PSRIX recordings, B1 was only recorded in the raw voltages.

At the 32  $\mu$ s time resolution of the data products we use here, all bursts except B2 are single-component events, with fluences ranging from 0.13–0.71 Jy ms and total burst envelopes of only  $\sim 100 - 300 \mu$ s. We list the burst properties in Table 2. A detailed analysis of the burst properties and energetics is presented in Nimmo et al. (submitted).

For correlation, we used  $DM = 87.77 \text{ pc cm}^{-3}$ , which we derived from a first manual inspection of the bursts. To refine the DM for further analysis, however, we maximised the signal to noise ratio (S/N) of a very narrow spike in B3 (Figure 1g, Nimmo et al., submitted) and find  $DM = 87.7527 \pm 0.0003 \text{ pc cm}^{-3}$ . This value is comparable to, but formally deviates from  $DM = 87.818 \pm 0.007 \text{ pc cm}^{-3}$  found by [Bhardwaj et al. \(2021\)](#), where a weighted average of three bursts was used. Possible explanations for this discrepancy are the lack of short-timescale structure in the bursts found by [Bhardwaj et al. \(2021\)](#), the potential for non-dispersive time-frequency drifting ([Hessels et al. 2019](#)) or a time-variable DM. Nimmo et al. (submitted) present a full spectro-polarimetric analysis of the bursts using data products with much higher temporal resolution (31.25 ns to 8  $\mu$ s).

Figure 2 displays the dirty maps (i.e. the inverse Fourier Transform of the visibilities without applying any deconvolution, i.e. ‘CLEANing’) of the bursts that were detectable in the correlated data, using a natural weighting of the data. B1 was too faint to produce a useful image, and we therefore exclude it from the localisation analysis. The individual correlated data sets span only the width of their respective

gates (Table 2). Given the rather sparse arrays in each run, this results in elongated fringe patterns in the images, hindering an unambiguous localisation. Therefore, as also shown in Figure 2, we create data sets that are combinations of the visibilities from B3 and B4, and also from B2, B3, and B4. In this way we can identify an overlapping region that we fit with an elliptical Gaussian. We fit this component to the envelope of the fringe patterns for B3, B4, and the combination of B2, B3, and B4. The first two cases yielded an elongated Gaussian component that only provided an accurate position in one dimension, while the later one resulted in a better localisation (see Figure 2). The final coordinates (J2000) of FRB 20200120E are  $\text{RA} = 9^{\text{h}}57^{\text{m}}54.68^{\text{s}} \pm 0.29^{\text{s}}$   $\text{Dec} = 68^{\circ}49'0.8'' \pm 0.4''$ . We note that the quoted uncertainties are significantly larger than the synthesized beams ( $\sim 20 \text{ mas}$ ), and the statistical uncertainties related to phase-referencing errors and position uncertainty of the phase calibrator are negligible (all of them  $\lesssim 1 \text{ mas}$ ). These final values are thus dominated by the fringe patterns, as mentioned before. These coordinates coincide with the location of the globular cluster [PR95] 30244 ([Perelmuter et al. 1995](#)), which is part of the M81 globular cluster system ([Perelmuter & Racine 1995; Nantais & Huchra 2010](#)).

### 3.2. *Deep radio imaging of the region*

In addition to imaging the bursts themselves, we also created a deep continuum image from the combination of the data from both VLBI observations. The resulting map (Figure 3a) has a rms background of  $23 \mu\text{Jy beam}^{-1}$ . We find no persistent source at the location of FRB 20200120E above a  $5\sigma$  confidence level. Also shown in Figure 3 are the continuum images obtained with the VLA at 1.5 GHz and at 340 MHz. These maps have noise levels of  $6.5 \mu\text{Jy beam}^{-1}$  and  $320 \mu\text{Jy beam}^{-1}$ , respectively. Also here, no persistent source is detected at the position of FRB 20200120E in either of the images. For a 1.5 GHz radio flux density limit of  $20 \mu\text{Jy}$  ( $3\sigma$ ) and a distance of 3.6 Mpc, we limit the radio luminosity  $L_{\nu} < 3.1 \times 10^{23} \text{ erg s}^{-1} \text{ Hz}^{-1}$ . This luminosity limit is  $\sim 10^3$  times lower than that of any other extragalactic FRB ([Marcote et al. 2020](#)) and almost  $10^6$  times lower than the radio luminosity of the persistent source in the vicinity of FRB 20121102A ([Marcote et al. 2017](#)).

In the data taken at 1.5 GHz (Figure 3b), we did identify two sources with peak brightness of  $110 \mu\text{Jy beam}^{-1}$  and  $73 \mu\text{Jy beam}^{-1}$ , and offset by 6'' and 9'', respectively. The projected density of radio sources of this brightness is roughly 1000 to 3000 per square degree ([Condon et al. 2012](#)). Therefore, we expect between 1–3 sources within 1' of FRB 20200120E by chance. The closer of the two nearby radio sources is within 0.2'' of a PS1 source with  $i = 21.3$  mag. This host galaxy has a photometric redshift in the PS1 STRM catalogue ([Beck et al. 2021](#)) of  $0.67 \pm 0.2$ ,

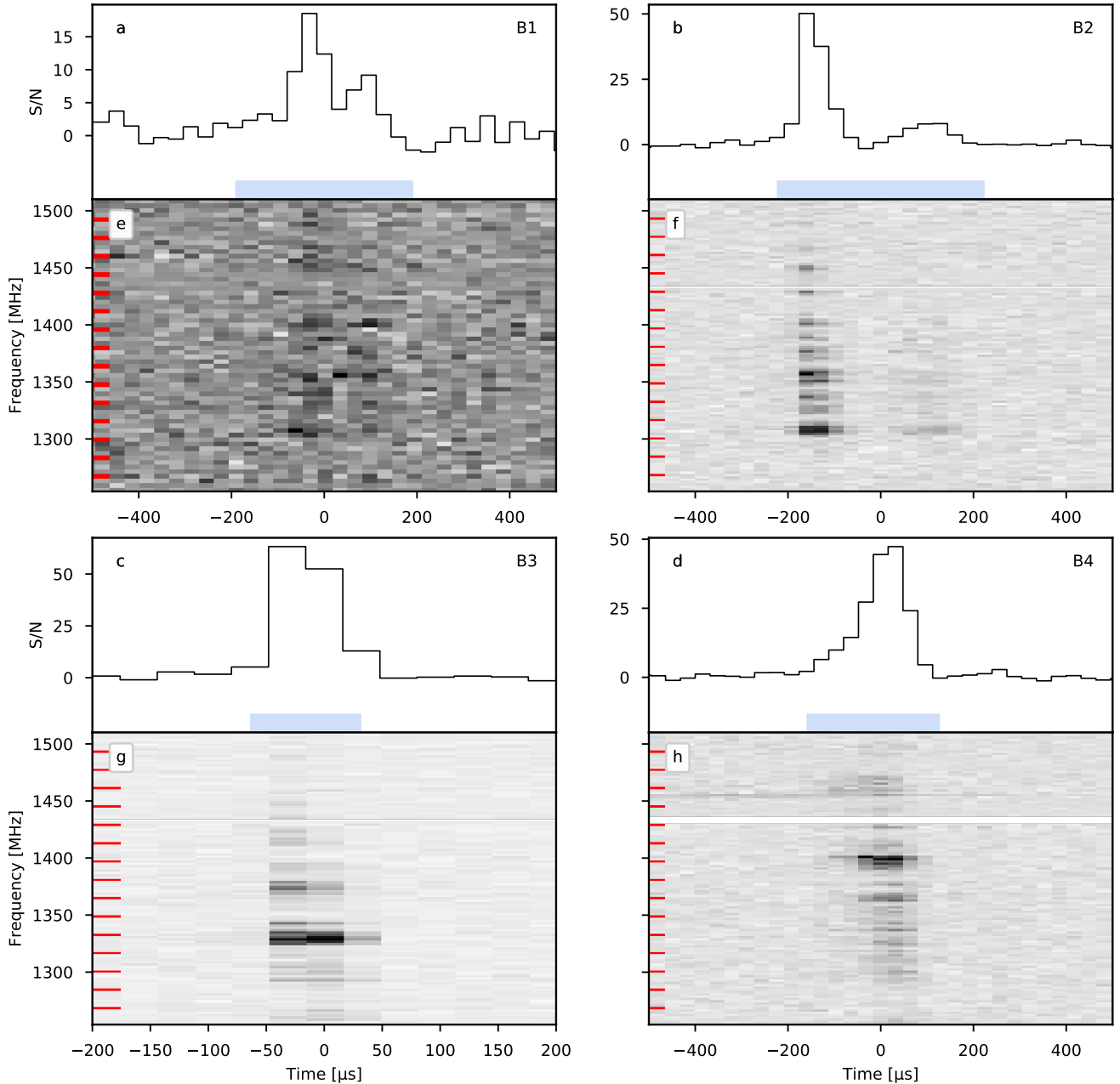


**Figure 1. Dispersion-corrected time series and dynamic spectra of the four FRB 20200120E bursts detected with Effelsberg during an *ad hoc* VLBI campaign.** Frequency-averaged time series of the bursts are displayed in panels a-d. The top right corner of each panel shows the burst name used in this work. The blue-coloured bars highlight the  $\pm 2\sigma$  burst width used to measure the burst fluence. The dynamic spectra of each burst are shown in panels e-h. The red marks represent the edges of the subbands. Data that have been removed due to contamination by radio frequency interference have not been plotted. In all panels the data are plotted with 32  $\mu$ s and 2 MHz time and frequency resolution, respectively (with the exception of B1 which is plotted with 4 MHz frequency resolution).

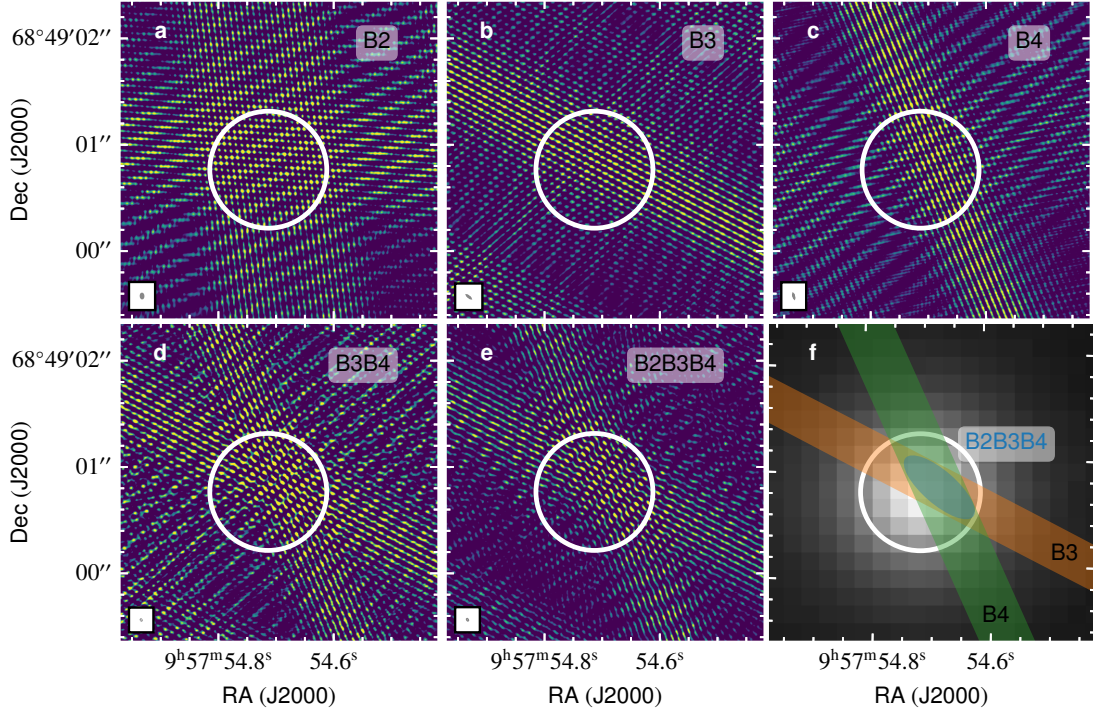


**Figure 2. Localisation plots for FRB 20200120E.** Normalised dirty images of the individual bursts (**a-c**) and combination of B3+B4 and B2+B3+B4 (**d-e**) produced by applying a natural weighting to the data. For visualisation purposes we clip the colour scale at zero, i.e. only positive peaks are displayed. The white circles are centred on the location of the globular cluster [PR95] 30244 as derived from the Subaru image in Figure 4. Their size indicates the region that contains 90% of the globular cluster's emission. The synthesized beams of each image are displayed as grey ellipses in the bottom left corner of each panel. **f:** The resulting localisation as derived from the combined data sets with respect to the optical Subaru image of the region (greyscale background, Figure 4). The green and orange stripes model the fringe distribution of B3 and B4, respectively; the blue ellipse indicates the localisation region as derived from combining the data of B2, B3, and B4. The resulting coordinates (J2000) for FRB 20200120E are RA =  $9^{\text{h}}57^{\text{m}}54.68^{\text{s}} \pm 0.29^{\text{s}}$  Dec =  $68^{\circ}49'0.8'' \pm 0.4''$ . See text for details.

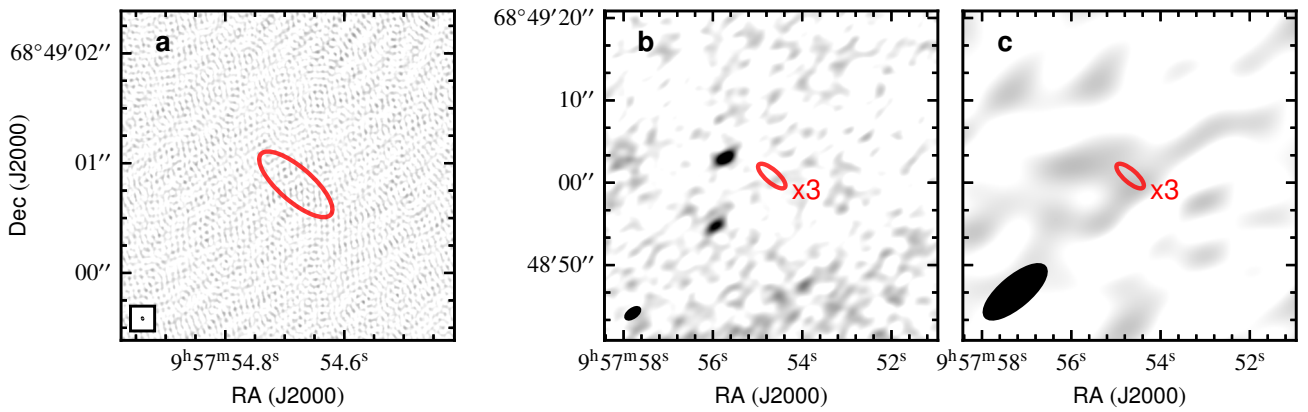


**Figure 3. Continuum maps in the field around FRB 20200120E.** **a:** 1.4-GHz EVN continuum image after combining the two epochs (EK048B and EK048C); **b:** 1.5-GHz *Realfast*, and **c:** 340-MHz VLITE continuum image. The red circle indicates the  $1\sigma$  (for EVN) and  $3\sigma$  (for *Realfast*, VLITE) uncertainty region of FRB 20200120E. Note the different scales amongst the three panels. We clip all values below zero and above  $138 \mu\text{Jy beam}^{-1}$  (EVN),  $50 \mu\text{Jy beam}^{-1}$  (*Realfast*) and  $3 \text{mJy beam}^{-1}$  (VLITE) for visualisation purposes. The black ellipse in the bottom left corner of each panel indicates the synthesised beam size and position angle.

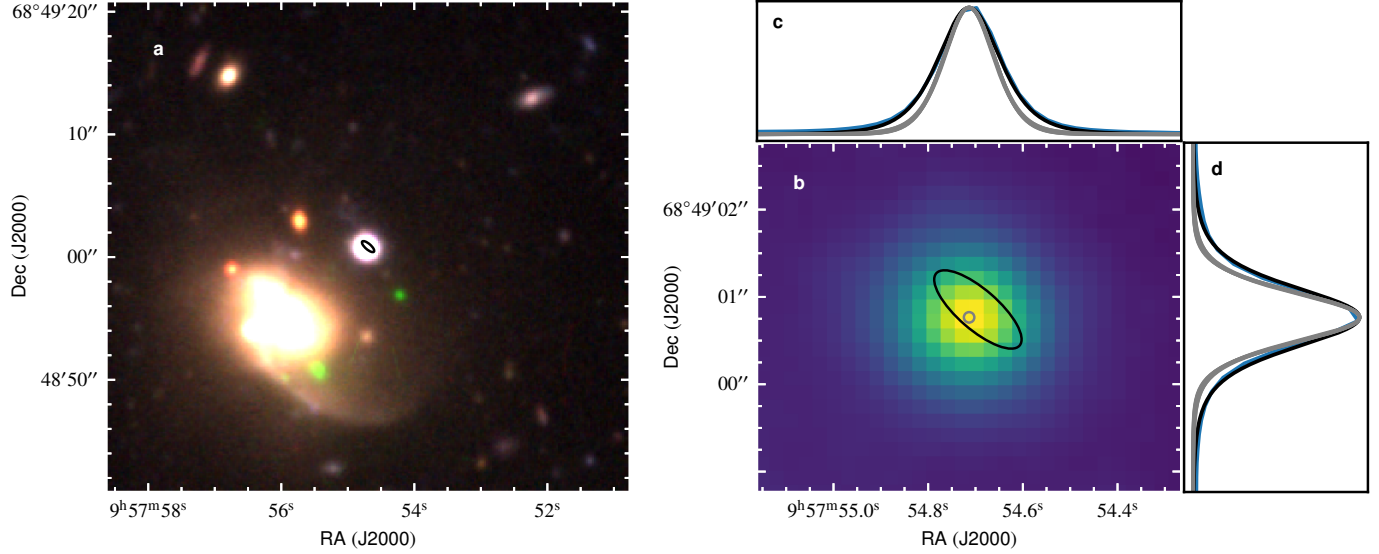


**Figure 4.** Optical images of FRB 20200120E’s field. Left (**a**):  $40'' \times 40''$   $g'$ ,  $r'$ , and  $i'$  band image of [PR95] 30244 acquired with Hyper Suprime-cam. The black ellipse is centred at the location of FRB 20200120E and its size represents the  $3\sigma$  uncertainty region. In panel **b** we show the zoomed in  $r'$  band image of [PR95] 30244. The grey circle represents the estimated position of the centre of [PR95] 30244 and its  $1\sigma$  uncertainty. The black ellipse is the same as in panel **a**. Panels **c** and **d** show cross-sections of the brightness distribution of the cluster (blue solid lines). Indicated in solid grey lines is the PSF as measured from stars in the images. It is obvious that [PR95] 30244 is resolved.

**Table 2.** Burst properties.

Burst	MJD <sup>a</sup>	Fluence [Jy ms] <sup>b</sup>	Peak S/N	Peak Flux Density [Jy] <sup>b</sup>	Width <sup>c</sup> [ $\mu$ s]	Gate width <sup>d</sup> [ $\mu$ s]
B1	59265.88304437179	$0.13 \pm 0.03$	18.6	$4.5 \pm 0.9$	$156 \pm 1$	290
B2	59265.88600912486	$0.63 \pm 0.12$	54.9	$6.6 \pm 1.3$	$62 \pm 1, 93 \pm 0.5$ <sup>e</sup>	150
B3	59280.69618745651	$0.52 \pm 0.10$	64.5	$7.8 \pm 1.6$	$47 \pm 0.1$	126
B4	59280.80173397988	$0.71 \pm 0.14$	47.0	$5.7 \pm 1.2$	$117 \pm 1$	386

<sup>a</sup> Corrected to the solar system barycentre to infinite frequency assuming a dispersion measure of  $87.75 \text{ pc cm}^{-3}$ , reference frequency 1502 MHz and dispersion constant of  $1/(2.41 \times 10^{-4}) \text{ MHz}^2 \text{ pc}^{-1} \text{ cm}^3 \text{ s}$ .

<sup>b</sup> The times quoted are dynamical times (TDB).

<sup>c</sup> The receiver temperature of Effelsberg is 20 K and the telescope gain is  $1.54 \text{ K Jy}^{-1}$ . We additionally consider a sky background temperature of 0.8 K, by extrapolating from the 408 MHz map (Remazeilles et al. 2015), using a spectral index of  $-2.7$  (Reich & Reich 1988), and 3 K from the cosmic microwave background (Mather et al. 1994). We take a conservative 20 % error on these measurements, arising due to the uncertainty in the Effelsberg receiver temperature and gain.

<sup>d</sup> Defined as  $1/\sqrt{2}$  multiplied by the full-width at half-maximum of the autocorrelation function (ACF).

Note we use the  $\pm 2\sigma$  burst width region to determine the burst fluence (see Nimmo et al. (submitted) for details).

<sup>e</sup> Width of the gate used for the interferometric correlation of each burst.

<sup>f</sup> Width per burst component.

so it is most likely a background galaxy. The other identified radio source has no PS1 counterpart. We note that none of these two sources exhibit significant compact emission on milliarcsecond scales.

### 3.3. Optical association and chance coincidence probability

Figure 4a shows the location of FRB 20200120E with respect to the globular cluster [PR95] 30244 in a combined three-colour image made with  $i'$ ,  $r'$ , and  $g'$  filters mapped to

red, green, and blue channels, respectively. The galaxy at the bottom-left of [PR95] 30244 is a background SDSS galaxy at redshift  $z = 0.194$ , i.e. at a  $z$  much larger than the maximal possible value ( $z < 0.03$ ) estimated by Bhardwaj et al. (2021).

We performed radial fits to the brightness distribution of [PR95] 30244 with the Moffat profile (Moffat 1969) in both RA and Dec for all three bands after fitting and subtracting a bilinearly varying background (to account for the presence

**Table 3.** Notable properties of [PR95] 30244.

Property	Value	Reference
Metallicity $\log[Z/Z_\odot]$	$-1.79^{+0.84}_{-0.85}$	this work
Metallicity [Fe/H]	$-1.83^{+0.86}_{-0.87}$	this work
Stellar mass $\log[M/M_\odot]$	$5.78^{+0.19}_{-0.22}$	this work
Effective radius ( $R_{\text{eff}}$ ; kpc)	3.7	this work
Mass-weighted age (Gyr)	$9.13^{+3.27}_{-4.18}$	this work
$(u - r)_0^a$ (AB mag)	1.96(2)	Alam et al. (2015a)
E(V-B) <sup>b</sup>	$0.19^{+0.09}_{-0.10}$	this work
$\sigma_r$ (km s <sup>-1</sup> )	22	this work
Absolute r-band mag. (AB)	-8.4	-
Luminosity distance (Mpc)	3.6	Karachentsev (2005)

<sup>a</sup> Milky Way extinction is corrected using the reddening map by Schlegel et al. (1998).

<sup>b</sup> Using  $R_v = 3.1$ .

of the background galaxy). The average position of the centroid of [PR95] 30244 is RA =  $9^{\text{h}}57^{\text{m}}54.7135^{\text{s}}$   $\pm$  7 mas, Dec =  $68^\circ49'0.766''$   $\pm$  4 mas (statistical). These coordinates are consistent with the ones listed in Perelmutter et al. (1995) but disagree with the ones in Nantais & Huchra (2010)<sup>1</sup>. We measured the full-width at half maximum (FWHM; ‘seeing’) of the coadded  $i'$ ,  $r'$ , and  $g'$  images to be 0'.63, 0'.57, and 0'.62, respectively, using profile fits to bright, isolated stars. The brightness distribution of [PR95] 30244 has an FWHM of 0'.77, 0'.70, and 0'.75 in the same three images. Subtracting the FWHMs of the isolated stars in quadrature, we estimate that the intrinsic FWHM of [PR95] 30244 is about 0'.42, corresponding to about 7.4 pc at a distance of 3.63 Mpc.

Figure 4b shows a zoomed in image centred on [PR95] 30244 with the FRB 20200120E location denoted by a black circle. The centre of the FRB location is 135 mas offset from the centre of [PR95] 30244. Given the astrometric uncertainty of the FRB localisation (400 mas) and the optical image registration error (60 mas), FRB 20200120E is consistent with being located at the centre of [PR95] 30244.

Bhardwaj et al. (2021) argued that, if FRB 20200120E is extragalactic, it would not lie beyond M81 based on its low DM. They also identified several known sources associated with M81, including [PR95] 30244, that could be associated with the FRB. Here we quantitatively assess the association of FRB 20200120E and [PR95] 30244 by estimating the probability of chance coincidence for an M81 globular cluster in the FRB localisation region. Following the prescription of Bloom et al. (2002), we use a circular localisation region with a radius ( $R$ ) =  $\max(2R_{\text{eff}}$  of [PR95] 30244,

maximum seeing-limited size of [PR95] 30244 in the Hyper Suprime-images) = 0''.77 in our chance coincidence calculations. Perelmutter & Racine (1995) parameterized the projected areal number density ( $N_{\text{GC}}/\text{arcmin}^2$ ) of the M81 globular clusters as a function of their angular offset from M81 ( $r$ , in arcmin) as,  $\log_{10}(N_{\text{GC}}) = -2.07 \times \log_{10}(r) + 0.82 \pm 0.05$ , for  $0 \leq \log_{10}(r) \leq 1.4$ . At the offset of FRB 20200120E from M81 (19.6'),  $N_{\text{GC}} = 0.014 \text{ arcmin}^{-2} \approx 3.8 \times 10^{-6} \text{ arcsec}^{-2}$ . Assuming a Poisson distribution of M81 globular clusters at  $r = 19.6'$ , the probability of finding at least one globular cluster by chance within a radius  $R$  is given by  $P_{\text{cc}} = 1 - \exp(-\pi R^2 N_{\text{GC}}) \approx 7 \times 10^{-6}$ . A more conservative estimate of  $P_{\text{cc}}$  can be derived by assuming that all the predicted  $300 \pm 100$  M81 globular clusters (Harris et al. 2013) are uniformly distributed within the angular area of radius = 19.6' so that  $N_{\text{GC}} = 4.6 - 9.2 \times 10^{-5}$ , and consequently  $P_{\text{cc}} = 0.85 - 1.7 \times 10^{-4}$ . From such a very low  $P_{\text{cc}}$  value, we conclude that the association of FRB 20200120E and [PR95] 30244 is robust.

### 3.4. Modelling of [PR95] 30244

To estimate important physical properties of [PR95] 30244, such as its stellar mass, metallicity, stellar population age and V-band extinction, we used the Prospector code (Leja et al. 2017; Johnson et al. 2019) for stellar population inference. We modelled the SDSS photometry of [PR95] 30244 and fit a five-parameter ‘delayed-tau’ model for the star formation rate  $\text{SFR}(t) \propto t \exp(-t/\tau)$ , where  $t$  is the time since the formation epoch of the galaxy, and  $\tau$  is the characteristic decay time of the star-formation history of [PR95] 30244 (Simha et al. 2014; Carnall et al. 2019). The model and assumed prior of each free-parameter are discussed in Appendix A. The best-fit spectral energy distribution (SED) profile of [PR95] 30244 is shown in Figure 6. Prospector also enables Markov Chain Monte Carlo (MCMC) sampling of the posterior to estimate uncertainty in the best-fit values of the physical properties of [PR95] 30244, which are listed in Table 3. Using the following relation from Bertelli et al. (1994),  $[\text{Fe}/\text{H}] = 1.024 \times \log(Z/Z_\odot)$ , we estimate the [Fe/H] of [PR95] 30244 =  $-1.83^{+0.86}_{-0.87}$ , which is in good agreement with the value estimated by Perelmutter et al. (1995). We can get an estimate of the velocity dispersion ( $\sigma_r$ ) of [PR95] 30244 using the virial theorem:  $\sigma_r \sim \sqrt{2GM/3R_{\text{eff}}}$ , where  $G$  is the gravitational constant. Using the M and  $R_{\text{eff}}$  values of [PR95] 30244 from Table 3, we estimate  $\sigma_r \sim 22 \text{ km s}^{-1}$ . Looking at the modelled physical properties, we conclude that [PR95] 30244 is an old ( $\sim 10$  Gyr), metal-poor globular cluster.

### 3.5. High energy counterparts

The X-ray count-rate in the source extraction region of the archival *Chandra* observations,  $4.4 \times 10^{-6}$

<sup>1</sup> Most likely, the minutes in RA as listed in Nantais & Huchra (2010) are incorrect.

counts s<sup>-1</sup> arcsec<sup>-2</sup>, is consistent with the background region rate of  $3.9 \times 10^{-6}$  counts s<sup>-1</sup> arcsec<sup>-2</sup>. To place a limit on an X-ray source at the location of FRB 20200120E we use the Bayesian method of Kraft et al. (1991), which results in a  $3\sigma$  0.5–10 keV source count rate upper limit of  $1 \times 10^{-3}$  counts s<sup>-1</sup>. Taking into account the spectral response for the off-axis location of the source (via an ancillary response file created by the CIAO tool `specextract`), and assuming a photoelectrically absorbed power-law source spectrum with a spectral index of  $\Gamma = 2$  and a hydrogen column density of  $N_{\text{H}} = 10^{21} \text{ cm}^{-2}$ , this count rate limit corresponds to a 0.5–10 keV absorbed flux upper limit of  $1 \times 10^{-14} \text{ erg cm}^{-2} \text{ s}^{-1}$ . At the distance of 3.6 Mpc, this results in a  $3\sigma$  0.5–10 keV luminosity upper limit of  $2 \times 10^{37} \text{ erg s}^{-1}$ . A detailed analysis of ongoing X-ray follow-up observations of the region will be presented in Pearlman et al. (in prep.).

No sources are reported at the location of M81 in any of the *Fermi*-LAT catalogues. The nearest catalogued source (at a separation of 52') is 4FGL J0955.7+6940, known to be associated with M82, whose high-energy properties are discussed in Abdo et al. (2010).

#### 4. DISCUSSION

As shown in §3, the chance alignment probability of FRB 20200120E with the globular cluster [PR95] 30244 is found to be low ( $< 1.7 \times 10^{-4}$ ), and hence we conclude that the two objects are robustly associated. In fact, the chance coincidence probability is dominated by the sky area covered by [PR95] 30244, as opposed to the precision of the burst localisation. In turn, the association of [PR95] 30244 with the M81 galactic system (Perelmutter & Racine 1995; Nantais & Huchra 2010) definitively establishes the extragalactic nature of FRB 20200120E. At a distance of only 3.6 Mpc, FRB 20200120E is thus conclusively proven to be the closest-known extragalactic FRB source, as suggested by Bhardwaj et al. (2021).

Within the context of FRB models that invoke a young, highly magnetized neutron star (NS) powered primarily by the decay of its magnetic field, i.e. a magnetar (e.g. Margalit & Metzger 2018; CHIME/FRB Collaboration et al. 2020), it is hard to reconcile FRB 20200120E's association with an old globular cluster using the standard core-collapse supernova formation channel of magnetars. Instead, such a magnetar would need to have been formed via accretion-induced collapse (AIC; Wang & Liu 2020, for a recent review) of a white dwarf (WD) or via merger-induced collapse (MIC) of a WD-WD, NS-WD or NS-NS binary (e.g. Giacomazzo & Perna 2013; Schwab et al. 2016; Zhong & Dai 2020) as are common in globular clusters (Hut et al. 1992; Pooley et al. 2003; Verbunt 2003), in particular at the core of such stellar systems (Prager et al. 2017). The most likely of the MIC-models is that of a merging WD-WD system as

those dominate the cores of globular clusters (Kremer et al. 2021), while a NS-NS progenitor system is less probable (Ye et al. 2020). In fact, Ye et al. (2019) estimate that a typical globular cluster with a total mass of  $\sim 2 \times 10^5 M_{\odot}$  can host 10 – 20 MSPs formed via AIC or MIC. At birth, such NSs would be extreme objects with high rotation rates and strong magnetic fields, capable of generating FRBs. We note that the metallicity limit ( $\log[\text{Fe}/\text{H}] > -0.6$ ) that Boyles et al. (2011) set for the formation of young NSs in globular clusters is much higher than the metallicity that we estimate for [PR95] 30244 ( $\log[\text{Fe}/\text{H}] = -1.83$ , Table 3). Nevertheless, non-recycled pulsars have been found towards some globular clusters (Lyne et al. 1996; Boyles et al. 2011, see also Hessels et al. 2015 for a review of pulsars in globular clusters). These young pulsars are formed at a comparable rate to MSPs in globular clusters, but they have much shorter active lifetimes (Myr versus Gyr). The lack of a persistent radio or X-ray source at the position of FRB 20200120E is expected in an AIC/MIC scenario, as any emission generated during collapse fades away on very short time scales (< 1 yr, Margalit et al. 2019). As no bright transient events are known from the direction of [PR95] 30244, the age of a potential magnetar is likely at least decades. Similarly, no persistent radio or X-ray source would be expected if giant pulses from a recycled MSP were the origin of the FRBs detected from FRB 20200120E. A MSP with rotation period  $P = 0.8 \text{ ms}$ , period derivative  $\dot{P} = 4 \times 10^{-18} \text{ s s}^{-1}$  (i.e. magnetic field strength  $B = 6 \times 10^9 \text{ G}$  and characteristic age  $\tau = 3 \times 10^5 \text{ yr}$ ) would have a spin down luminosity  $\dot{E} = 1 \times 10^{39} \text{ erg s}^{-1}$ , sufficient to power giant pulse emission.

Alternatively, FRB 20200120E could be a compact binary system such as a tight WD-NS system in a pre-merger phase or a magnetised neutron star with a planetary companion (Mottez & Zarka 2014; Mottez et al. 2020). Similarly, a binary MSP with a strong magnetic field formed via AIC and that was subsequently spun-up via accretion (Abelmit & Li 2015; Ye et al. 2019) could act as an FRB engine. Such a system could also be observable as a low mass X-ray binary (LMXBs, Heinke et al. 2003), as would an accreting black hole (BH). LMXBs in the hard state typically have X-ray and radio luminosities of up to  $10^{38} \text{ erg s}^{-1}$  and  $10^{32} \text{ erg s}^{-1}$ , respectively (Gallo et al. 2018). In such an LMXB model with either a NS or a BH, the radio bursts could be generated via magnetic reconnections in a relativistic jet or where the jet shocks with the surrounding medium and creates a synchrotron maser (Sridhar et al. 2021). Except for the most luminous LMXBs, our observations cannot rule out such systems. However, none of the  $\sim 200$  Galactic LMXBs has been seen to generate FRBs.

In some cases, ultra-luminous X-ray sources (ULXs, Kaaret et al. 2017) have been shown to be NSs accreting at hyper-Eddington rates (Bachetti et al. 2014), though some

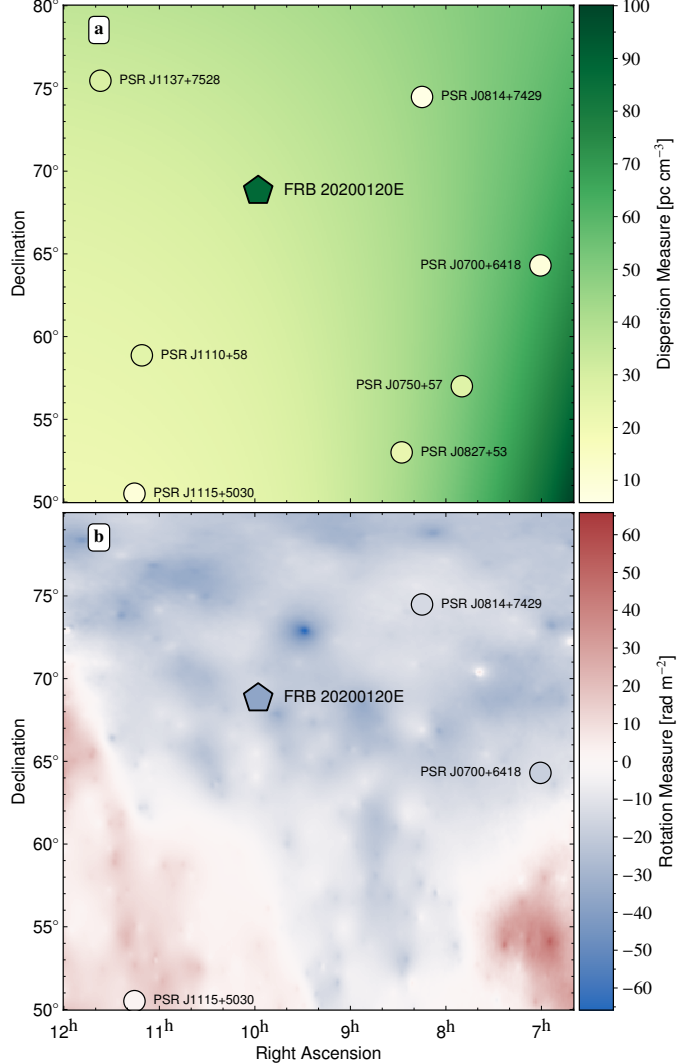


**Figure 5. Dispersion measure (DM) and rotation measure (RM) maps around FRB 20200120E:** Panel **a** shows the expected Galactic DM contribution (background) according to the YMW16 model (disk contribution only, Yao et al. 2017), the DM of FRB 20200120E (pentagon) and the DMs of known pulsars from the ATNF Pulsar Catalogue in this field (circles, Hobbs et al. 2004). Panel **b** shows the physical Galactic Faraday depth  $\phi_g$  (background, Hutschenreuter et al. 2021), the RM of FRB 20200120E (pentagon) and galactic pulsars with a known RM (circles). We assume that the RM of FRB 20200120E is  $-36.9 \text{ rad m}^{-2}$  (Bhardwaj et al. 2021, also see Nimmo et al. (submitted) for details)

may be systems with a more massive BH primary (Webb et al. 2012). We note that ULXs have been associated with extragalactic globular clusters (Dage et al. 2020) but such systems are ruled out by our X-ray limit unless their luminosity varies in time by more than two orders of magnitude.

There no known X-ray sources within  $\sim 2'$  of FRB 20200120E's position and the closest-known gamma-ray source in the *Fermi*-LAT (4FGL-DR2) catalogue (4FGL J0955.7+6940) is offset by 52' from our localisation. Nonetheless, if FRB 20200120E is an accreting system with a jet, the brightness of any persistent radio, X-ray, or gamma-ray counterpart could be time variable and depend on the accretion rate or precession phase of the jet. We point out that globular clusters are known to be gamma-ray sources

due to the emission from non-thermal processes in the magnetospheres of MSPs. de Menezes et al. (2019) report the detection of 23 globular clusters using the *Fermi*-LAT. However, even the most luminous known Galactic GC (Terzan5), whose luminosity is  $(42.4 \pm 1.5) \times 10^{34} \text{ erg s}^{-1}$  in the 0.1–100 GeV energy range, would have a gamma-ray flux of only  $(2.00 \pm 0.07) \times 10^{-16} \text{ erg cm}^{-2} \text{ s}^{-1}$  at the distance of M81. This is nearly 3 orders of magnitude dimmer than the faintest source detected in the 4FGL-DR2 catalogue.

Since FRB 20200120E is extragalactic, its dispersive delay is probing the full extent of the Milky Way ISM ( $\text{DM}_{\text{ISM}}^{\text{MW}}$ ) and halo ( $\text{DM}_{\text{Halo}}^{\text{MW}}$ ) along this line of sight. There are also extragalactic contributions from the intergalactic medium  $\text{DM}_{\text{IGM}}$  and the host galaxy ( $\text{DM}_{\text{M81}}$ ), leading to the total

observed  $\text{DM} = \text{DM}_{\text{ISM}}^{\text{MW}} + \text{DM}_{\text{Halo}}^{\text{MW}} + \text{DM}_{\text{IGM}} + \text{DM}_{\text{M81}}$ . The intergalactic medium between the Milky Way and M81 contributes on the order of  $\text{DM}_{\text{IGM}} = 1 \text{ pc cm}^{-3}$  (according to the average Macquart relation; Macquart et al. 2020). To estimate  $\text{DM}_{\text{M81}}$ , we only consider the contribution from the halo of M81, as both the M81 disk and the globular cluster make negligible contributions to the measured DM. Bhardwaj et al. (2021) estimated the M81 halo DM contribution to be  $\sim 15\text{--}50 \text{ pc cm}^{-3}$  depending on the choice of a halo density profile and baryon fraction in the M81 halo. For the Galactic contribution, models of the Milky Way ISM predict  $\text{DM}_{\text{ISM}}^{\text{MW}} = 30\text{--}40 \text{ pc cm}^{-3}$  in this direction (with a shallow spacial gradient in the region, Figure 5; Cordes & Lazio 2002; Yao et al. 2017). Using these estimates, we limit the Milky Way halo contribution to the FRB sight-line, which is poorly constrained by current observations (Keating & Pen 2020), to  $\text{DM}_{\text{Halo}}^{\text{MW}} = \text{DM} - \text{DM}_{\text{ISM}}^{\text{MW}} - \text{DM}_{\text{IGM}} - \text{DM}_{\text{M81}} \lesssim 32\text{--}42 \text{ pc cm}^{-3}$ . This is well in line with the models of Yamasaki & Totani (2020), which predict  $\text{DM}_{\text{Halo}}^{\text{MW}} = 10\text{--}30 \text{ pc cm}^{-3}$ , but lower than predicted in other models (e.g. Prochaska & Zheng 2019).

Similar considerations are also applicable for the rotation measure  $\text{RM} = -36.9 \text{ rad m}^{-2}$  as determined in the companion paper by Nimmo et al. (submitted) and by Bhardwaj et al. (2021). The Galactic contribution along the line of sight to FRB 20200120E is  $\text{RM} = -16.9 \pm 4.3 \text{ rad m}^{-2}$  (Figure 5; Hutschenreuter et al. 2021). The contribution of the IGM is most likely minor, leaving only the MW halo, the M81 halo and the local environment of FRB 20200120E as contributing sources. The RMs of the MW- and M81-halo are likely small ( $|\text{RM}| < 20 \text{ rad m}^{-2}$ ), constraining  $\text{RM}_{\text{Local}}$  to the range  $[+20, -60] \text{ rad m}^{-2}$ . This is comparable to FRB 20180916B ( $\text{RM} = -115 \text{ rad m}^{-2}$ , CHIME/FRB Collaboration et al. 2019) but three orders of magnitude lower than the RM of FRB 20121102A ( $> 1.3 \times 10^5 \text{ rad m}^{-2}$ ; Michilli et al. 2018b). This indicates that models of FRB sources do not necessarily require extreme magneto-ionic environments, unless the magnetic fields along the line of sight to both FRB 20200120E and FRB 20180916B are strongly tangled to result in a low net RM. More likely though, FRB 20121102A resides in a very different environment giving rise to its observed properties.

The persistent source supposedly associated with FRB 20121102A has been hypothesised to either be a BH accreting at a low rate (e.g. Marcote et al. 2017) or the remnant of a superluminous supernova (SLSN) that is powered by a magnetar or rapidly spinning NS (e.g. Marcote et al. 2017; Margalit & Metzger 2018). Assuming a common SLSN formation channel for young magnetars powering FRB emission, the lack of a persistent source in the surrounding of FRB 20180916B (Marcote et al. 2020) can be explained by different ages, i.e. FRB 20180916B might be older than

FRB 20121102A and, thus, the SNR would have faded away. However, a standard core-collapse SN is excluded as a formation channel for FRB 20200120E. So in case FRB 20121102A, FRB 20180916B, and FRB 20200120E have the same formation channel, e.g. AIC in a WD-WD binary system, the only difference between the three sources is the environment they reside in. Alternatively, if FRB 20121102A was indeed formed in a SLSN, this possibly indicates different formation channels for FRB sources.

## ACKNOWLEDGEMENTS

We would like to thank the directors and staff at the various participating stations for allowing us to use their facilities and running the observations. The European VLBI Network is a joint facility of independent European, African, Asian, and North American radio astronomy institutes. Scientific results from data presented in this publication are derived from the following EVN project code: EK048. This work was also based on simultaneous EVN and PSRIX data recording observations with the 100-m telescope of the MPIfR (Max-Planck-Institut für Radioastronomie) at Effelsberg, and we thank the local staff for this arrangement. We would like to express our gratitude to Willem van Straten for modifying the DSPSR software package to fit our needs. We appreciate helpful discussions about magnetar formation scenarios in a globular cluster environment with E. P. J. van den Heuvel. A.B.P is a McGill Space Institute (MSI) Fellow and a Fonds de Recherche du Quebec - Nature et Technologies (FRQNT) postdoctoral fellow. B.M. acknowledges support from the Spanish Ministerio de Economía y Competitividad (MINECO) under grant AYA2016-76012-C3-1-P and from the Spanish Ministerio de Ciencia e Innovación under grants PID2019-105510GB-C31 and CEX2019-000918-M of ICCCUB (Unidad de Excelencia “María de Maeztu” 2020-2023). Basic research in radio astronomy at NRL is funded by 6.1 Base funding. Construction and installation of VLITE was supported by the NRL Sustainment Restoration and Maintenance fund. C.J.L. acknowledges support from the National Science Foundation Grant 2022546. C.L. was supported by the U.S. Department of Defense (DoD) through the National Defense Science & Engineering Graduate Fellowship (NDSEG) Program. D.M. is a Banting Fellow. E.P. acknowledges funding from an NWO Veni Fellowship. F.K. acknowledges support from the Swedish Research Council. FRB research at UBC is supported by an NSERC Discovery Grant and by the Canadian Institute for Advanced Research. J.P.Y. is supported by the National Program on Key Research and Development Project (2017YFA0402602). K.S. is supported by the NSF Graduate Research Fellowship Program. K.W.M. is supported by an NSF Grant (2008031). M.B. is supported by an FRQNT Doctoral Research Award. N.W. acknowledges support from the National Natural Science Founda-

tion of China (Grant 12041304 and 11873080) P.S. is a Dunlap Fellow and an NSERC Postdoctoral Fellow. The Dunlap Institute is funded through an endowment established by the David Dunlap family and the University of Toronto. Part of this research was carried out at the Jet Propulsion Laboratory, California Institute of Technology, under a contract with the National Aeronautics and Space Administration. The NANOGrav project receives support from National Science Foundation (NSF) Physics Frontiers Center award number 1430284. The Dunlap Institute is funded through an endowment established by the David Dunlap family and the University of Toronto. B.M.G. acknowledges the support of the Natural Sciences and Engineering Research Council of Canada (NSERC) through grant RGPIN-2015-05948, and of the Canada Research Chairs program. The National Radio Astronomy Observatory is a facility of the National Science Foundation operated under cooperative agreement by Associated Universities, Inc. SMR is a CIFAR Fellow and is supported by the NSF Physics Frontiers Center award 1430284. This work is based in part on observations carried out using the 32-m radio telescope operated by the Institute of Astronomy of the Nicolaus Copernicus University in Toruń (Poland) and supported by a Polish Ministry of Science and Higher Education SpUB grant. V.B. acknowledges support from the Engineering Research Institute Ventspils International Radio Astronomy Centre (VIRAC). V.M.K. holds the Lorne Trottier Chair in Astrophysics &

Cosmology and a Distinguished James McGill Professorship and receives support from an NSERC Discovery Grant and Herzberg Award, from an R. Howard Webster Foundation Fellowship from the Canadian Institute for Advanced Research (CIFAR), and from the FRQNT Centre de Recherche en Astrophysique du Québec. We receive support from Ontario Research Fund—research Excellence Program (ORFRE), Natural Sciences and Engineering Research Council of Canada (NSERC) [funding reference number RGPIN-2019-067, CRD 523638-201, 555585-20], Canadian Institute for Advanced Research (CIFAR), Canadian Foundation for Innovation (CFI), the National Science Foundation of China (Grants No. 11929301), Simons Foundation, Thoth Technology Inc, and Alexander von Humboldt Foundation. Computations were performed on the SOSCIP Consortium’s [Blue Gene/Q, Cloud Data Analytics, Agile and/or Large Memory System] computing platform(s). SOSCIP is funded by the Federal Economic Development Agency of Southern Ontario, the Province of Ontario, IBM Canada Ltd., Ontario Centres of Excellence, Mitacs and 15 Ontario academic member institutions. Based [in part] on data collected at Subaru Telescope, which is operated by the National Astronomical Observatory of Japan. The National Radio Astronomy Observatory (NRAO) is a facility of the National Science Foundation operated under cooperative agreement by Associated Universities, Inc. AIPS is a software package produced and maintained by the National Radio Astronomy Observatory (NRAO).

## REFERENCES

- Abdo, A. A., Ackermann, M., Ajello, M., et al. 2010, ApJL, 709, L152, doi: [10.1088/2041-8205/709/2/L152](https://doi.org/10.1088/2041-8205/709/2/L152)
- Ablimit, I., & Li, X.-D. 2015, ApJ, 800, 98, doi: [10.1088/0004-637X/800/2/98](https://doi.org/10.1088/0004-637X/800/2/98)
- Agarwal, D., Aggarwal, K., Burke-Spolaor, S., Lorimer, D. R., & Garver-Daniels, N. 2020, MNRAS, 497, 1661, doi: [10.1093/mnras/staa1856](https://doi.org/10.1093/mnras/staa1856)
- Alam, S., Albareti, F. D., Allende Prieto, C., et al. 2015a, ApJS, 219, 12, doi: [10.1088/0067-0049/219/1/12](https://doi.org/10.1088/0067-0049/219/1/12)
- . 2015b, ApJS, 219, 12, doi: [10.1088/0067-0049/219/1/12](https://doi.org/10.1088/0067-0049/219/1/12)
- Bachetti, M., Harrison, F. A., Walton, D. J., et al. 2014, Nature, 514, 202, doi: [10.1038/nature13791](https://doi.org/10.1038/nature13791)
- Bailes, M., Bassa, C. G., Bernardi, G., et al. 2021, MNRAS, 503, 5367, doi: [10.1093/mnras/stab749](https://doi.org/10.1093/mnras/stab749)
- Ballet, J., Burnett, T. H., Digel, S. W., & Lott, B. 2020, arXiv e-prints, arXiv:2005.11208. <https://arxiv.org/abs/2005.11208>
- Beck, R., Szapudi, I., Flewelling, H., et al. 2021, MNRAS, 500, 1633, doi: [10.1093/mnras/staa2587](https://doi.org/10.1093/mnras/staa2587)
- Bertelli, G., Bressan, A., Chiosi, C., Fagotto, F., & Nasi, E. 1994, A&AS, 106, 275
- Bethapudi, S., Kerr, M., Ray, P. S., et al. 2021, Research Notes of the American Astronomical Society, 5, 46, doi: [10.3847/2515-5172/abea22](https://doi.org/10.3847/2515-5172/abea22)
- Bhardwaj, M., Gaensler, B. M., Kaspi, V. M., et al. 2021, ApJL, 910, L18, doi: [10.3847/2041-8213/abeaa6](https://doi.org/10.3847/2041-8213/abeaa6)
- Bloom, J. S., Kulkarni, S. R., & Djorgovski, S. G. 2002, AJ, 123, 1111, doi: [10.1086/338893](https://doi.org/10.1086/338893)
- Bochenek, C. D., Ravi, V., Belov, K. V., et al. 2020, Nature, 587, 59, doi: [10.1038/s41586-020-2872-x](https://doi.org/10.1038/s41586-020-2872-x)
- Bosch, J., Armstrong, R., Bickerton, S., et al. 2018, PASJ, 70, S5, doi: [10.1093/pasj/psx080](https://doi.org/10.1093/pasj/psx080)
- Boyles, J., Lorimer, D. R., Turk, P. J., et al. 2011, ApJ, 742, 51, doi: [10.1088/0004-637X/742/1/51](https://doi.org/10.1088/0004-637X/742/1/51)
- Carnall, A. C., Leja, J., Johnson, B. D., et al. 2019, ApJ, 873, 44, doi: [10.3847/1538-4357/ab04a2](https://doi.org/10.3847/1538-4357/ab04a2)
- CHIME/FRB Collaboration, Andersen, B. C., Bandura, K., et al. 2019, ApJL, 885, L24, doi: [10.3847/2041-8213/ab4a80](https://doi.org/10.3847/2041-8213/ab4a80)
- CHIME/FRB Collaboration, Andersen, B. C., Bandura, K. M., et al. 2020, Nature, 587, 54, doi: [10.1038/s41586-020-2863-y](https://doi.org/10.1038/s41586-020-2863-y)

- Choi, J., Dotter, A., Conroy, C., et al. 2016, ApJ, 823, 102, doi: [10.3847/0004-637X/823/2/102](https://doi.org/10.3847/0004-637X/823/2/102)
- Clarke, T. E., Kassim, N. E., Brisken, W., et al. 2016, in Society of Photo-Optical Instrumentation Engineers (SPIE) Conference Series, Vol. 9906, Ground-based and Airborne Telescopes VI, ed. H. J. Hall, R. Gilmozzi, & H. K. Marshall, 99065B, doi: [10.1117/12.2233036](https://doi.org/10.1117/12.2233036)
- Condon, J. J., Cotton, W. D., Fomalont, E. B., et al. 2012, ApJ, 758, 23, doi: [10.1088/0004-637X/758/1/23](https://doi.org/10.1088/0004-637X/758/1/23)
- Conroy, C., Gunn, J. E., & White, M. 2009, ApJ, 699, 486, doi: [10.1088/0004-637X/699/1/486](https://doi.org/10.1088/0004-637X/699/1/486)
- Cordes, J. M., & Lazio, T. J. W. 2002, arXiv e-prints, astro. <https://arxiv.org/abs/astro-ph/0207156>
- Cotton, W. D. 2008, PASP, 120, 439, doi: [10.1086/586754](https://doi.org/10.1086/586754)
- Dage, K. C., Zepf, S. E., Thygesen, E., et al. 2020, MNRAS, 497, 596, doi: [10.1093/mnras/staa1963](https://doi.org/10.1093/mnras/staa1963)
- de Menezes, R., Cafardo, F., & Nemmen, R. 2019, MNRAS, 486, 851, doi: [10.1093/mnras/stz898](https://doi.org/10.1093/mnras/stz898)
- Draine, B. T., & Li, A. 2007, ApJ, 657, 810, doi: [10.1086/511055](https://doi.org/10.1086/511055)
- Flewelling, H. A., Magnier, E. A., Chambers, K. C., et al. 2020, ApJS, 251, 7, doi: [10.3847/1538-4365/abb82d](https://doi.org/10.3847/1538-4365/abb82d)
- Foreman-Mackey, D., Hogg, D. W., Lang, D., & Goodman, J. 2013, PASP, 125, 306, doi: [10.1086/670067](https://doi.org/10.1086/670067)
- Freedman, W. L., Hughes, S. M., Madore, B. F., et al. 1994, ApJ, 427, 628, doi: [10.1086/174172](https://doi.org/10.1086/174172)
- Fruscione, A., McDowell, J. C., Allen, G. E., et al. 2006, in Society of Photo-Optical Instrumentation Engineers (SPIE) Conference Series, Vol. 6270, Society of Photo-Optical Instrumentation Engineers (SPIE) Conference Series, ed. D. R. Silva & R. E. Doxsey, 62701V, doi: [10.1117/12.671760](https://doi.org/10.1117/12.671760)
- Gallo, E., Degenaar, N., & van den Eijnden, J. 2018, MNRAS, 478, L132, doi: [10.1093/mnrasl/sly083](https://doi.org/10.1093/mnrasl/sly083)
- Garmire, G. P., Bautz, M. W., Ford, P. G., Nousek, J. A., & Ricker, George R., J. 2003, in Society of Photo-Optical Instrumentation Engineers (SPIE) Conference Series, Vol. 4851, X-Ray and Gamma-Ray Telescopes and Instruments for Astronomy., ed. J. E. Truemper & H. D. Tananbaum, 28–44, doi: [10.1117/12.461599](https://doi.org/10.1117/12.461599)
- Giacomazzo, B., & Perna, R. 2013, ApJL, 771, L26, doi: [10.1088/2041-8205/771/2/L26](https://doi.org/10.1088/2041-8205/771/2/L26)
- Greisen, E. W. 2003, AIPS, the VLA, and the VLBA, ed. A. Heck, Vol. 285, 109, doi: [10.1007/0-306-48080-8\\_7](https://doi.org/10.1007/0-306-48080-8_7)
- Harris, W. E., Harris, G. L. H., & Alessi, M. 2013, ApJ, 772, 82, doi: [10.1088/0004-637X/772/2/82](https://doi.org/10.1088/0004-637X/772/2/82)
- Heinke, C. O., Grindlay, J. E., Lugger, P. M., et al. 2003, ApJ, 598, 501, doi: [10.1086/378885](https://doi.org/10.1086/378885)
- Hessels, J., Possenti, A., Bailes, M., et al. 2015, in Advancing Astrophysics with the Square Kilometre Array (AASKA14), 47, <https://arxiv.org/abs/1501.00086>
- Hessels, J. W. T., Spitler, L. G., Seymour, A. D., et al. 2019, ApJL, 876, L23, doi: [10.3847/2041-8213/ab13ae](https://doi.org/10.3847/2041-8213/ab13ae)
- Hobbs, G., Manchester, R., Teoh, A., & Hobbs, M. 2004, in Young Neutron Stars and Their Environments, ed. F. Camilo & B. M. Gaensler, Vol. 218, 139. <https://arxiv.org/abs/astro-ph/0309219>
- Hut, P., McMillan, S., Goodman, J., et al. 1992, PASP, 104, 981, doi: [10.1086/133085](https://doi.org/10.1086/133085)
- Hutschenreuter, S., Anderson, C. S., Betti, S., et al. 2021, arXiv e-prints, arXiv:2102.01709. <https://arxiv.org/abs/2102.01709>
- Johnson, B. D., Leja, J. L., Conroy, C., & Speagle, J. S. 2019, Prospector: Stellar population inference from spectra and SEDs. <http://ascl.net/1905.025>
- Kaaret, P., Feng, H., & Roberts, T. P. 2017, ARA&A, 55, 303, doi: [10.1146/annurev-astro-091916-055259](https://doi.org/10.1146/annurev-astro-091916-055259)
- Karachentsev, I. D. 2005, AJ, 129, 178, doi: [10.1086/426368](https://doi.org/10.1086/426368)
- Keating, L. C., & Pen, U.-L. 2020, MNRAS, 496, L106, doi: [10.1093/mnrasl/slaa095](https://doi.org/10.1093/mnrasl/slaa095)
- Keimpema, A., Kettenis, M. M., Pogrebko, S. V., et al. 2015, Experimental Astronomy, 39, 259, doi: [10.1007/s10686-015-9446-1](https://doi.org/10.1007/s10686-015-9446-1)
- Kirsten, F., Snelders, M. P., Jenkins, M., et al. 2021, Nature Astronomy, 5, 414, doi: [10.1038/s41550-020-01246-3](https://doi.org/10.1038/s41550-020-01246-3)
- Kothes, R., Sun, X., Gaensler, B., & Reich, W. 2018, ApJ, 852, 54, doi: [10.3847/1538-4357/aa9e89](https://doi.org/10.3847/1538-4357/aa9e89)
- Kraft, R. P., Burrows, D. N., & Nousek, J. A. 1991, ApJ, 374, 344, doi: [10.1086/170124](https://doi.org/10.1086/170124)
- Kremer, K., Rui, N. Z., Weatherford, N. C., et al. 2021, arXiv e-prints, arXiv:2104.11751. <https://arxiv.org/abs/2104.11751>
- Law, C. J., Bower, G. C., Burke-Spolaor, S., et al. 2018, ApJS, 236, 8, doi: [10.3847/1538-4365/aab77b](https://doi.org/10.3847/1538-4365/aab77b)
- Law, C. J., Butler, B. J., Prochaska, J. X., et al. 2020, ApJ, 899, 161, doi: [10.3847/1538-4357/aba4ac](https://doi.org/10.3847/1538-4357/aba4ac)
- Lazarus, P., Karuppusamy, R., Graikou, E., et al. 2016, MNRAS, 458, 868, doi: [10.1093/mnras/stw189](https://doi.org/10.1093/mnras/stw189)
- Leja, J., Johnson, B. D., Conroy, C., van Dokkum, P. G., & Byler, N. 2017, ApJ, 837, 170, doi: [10.3847/1538-4357/aa5ffe](https://doi.org/10.3847/1538-4357/aa5ffe)
- Levenberg, K. 1944, Quarterly of applied mathematics, 2, 164
- Lyne, A. G., Manchester, R. N., & D’Amico, N. 1996, ApJL, 460, L41, doi: [10.1086/309972](https://doi.org/10.1086/309972)
- Macquart, J. P., Prochaska, J. X., McQuinn, M., et al. 2020, Nature, 581, 391, doi: [10.1038/s41586-020-2300-2](https://doi.org/10.1038/s41586-020-2300-2)
- Marcote, B., Paragi, Z., Hessels, J. W. T., et al. 2017, ApJL, 834, L8, doi: [10.3847/2041-8213/834/2/L8](https://doi.org/10.3847/2041-8213/834/2/L8)
- Marcote, B., Nimmo, K., Hessels, J. W. T., et al. 2020, Nature, 577, 190, doi: [10.1038/s41586-019-1866-z](https://doi.org/10.1038/s41586-019-1866-z)
- Margalit, B., Berger, E., & Metzger, B. D. 2019, ApJ, 886, 110, doi: [10.3847/1538-4357/ab4c31](https://doi.org/10.3847/1538-4357/ab4c31)
- Margalit, B., & Metzger, B. D. 2018, ApJL, 868, L4, doi: [10.3847/2041-8213/aaedad](https://doi.org/10.3847/2041-8213/aaedad)

- Mather, J. C., Cheng, E. S., Cottingham, D. A., et al. 1994, *ApJ*, 420, 439, doi: [10.1086/173574](https://doi.org/10.1086/173574)
- Mereghetti, S., Savchenko, V., Ferrigno, C., et al. 2020, *ApJL*, 898, L29, doi: [10.3847/2041-8213/aba2cf](https://doi.org/10.3847/2041-8213/aba2cf)
- Michilli, D., Hessels, J. W. T., Lyon, R. J., et al. 2018a, *MNRAS*, 480, 3457, doi: [10.1093/mnras/sty2072](https://doi.org/10.1093/mnras/sty2072)
- Michilli, D., Seymour, A., Hessels, J. W. T., et al. 2018b, *Nature*, 553, 182, doi: [10.1038/nature25149](https://doi.org/10.1038/nature25149)
- Miyazaki, S., Komiyama, Y., Nakaya, H., et al. 2012, in Society of Photo-Optical Instrumentation Engineers (SPIE) Conference Series, Vol. 8446, Ground-based and Airborne Instrumentation for Astronomy IV, ed. I. S. McLean, S. K. Ramsay, & H. Takami, 84460Z, doi: [10.1117/12.926844](https://doi.org/10.1117/12.926844)
- Moffat, A. F. J. 1969, *A&A*, 3, 455
- Mottez, F., & Zarka, P. 2014, *A&A*, 569, A86, doi: [10.1051/0004-6361/201424104](https://doi.org/10.1051/0004-6361/201424104)
- Mottez, F., Zarka, P., & Voisin, G. 2020, *A&A*, 644, A145, doi: [10.1051/0004-6361/202037751](https://doi.org/10.1051/0004-6361/202037751)
- Murase, K., Kashiyama, K., & Mészáros, P. 2016, *MNRAS*, 461, 1498, doi: [10.1093/mnras/stw1328](https://doi.org/10.1093/mnras/stw1328)
- Nantais, J. B., & Huchra, J. P. 2010, *AJ*, 139, 2620, doi: [10.1088/0004-6256/139/6/2620](https://doi.org/10.1088/0004-6256/139/6/2620)
- Offringa, A. R., McKinley, B., Hurley-Walker, N., et al. 2014, *MNRAS*, 444, 606, doi: [10.1093/mnras/stu1368](https://doi.org/10.1093/mnras/stu1368)
- Paxton, B., Marchant, P., Schwab, J., et al. 2015, *The Astrophysical Journal Supplement Series*, 220, 15
- Perelmutter, J.-M., Brodie, J. P., & Huchra, J. P. 1995, *AJ*, 110, 620, doi: [10.1086/117547](https://doi.org/10.1086/117547)
- Perelmutter, J.-M., & Racine, R. 1995, *AJ*, 109, 1055, doi: [10.1086/117341](https://doi.org/10.1086/117341)
- Petroff, E., Hessels, J. W. T., & Lorimer, D. R. 2019, *A&A Rv*, 27, 4, doi: [10.1007/s00159-019-0116-6](https://doi.org/10.1007/s00159-019-0116-6)
- Polisensky, E., Lane, W. M., Hyman, S. D., et al. 2016, *ApJ*, 832, 60, doi: [10.3847/0004-637X/832/1/60](https://doi.org/10.3847/0004-637X/832/1/60)
- Pooley, D., Lewin, W. H. G., Anderson, S. F., et al. 2003, *ApJL*, 591, L131, doi: [10.1086/377074](https://doi.org/10.1086/377074)
- Prager, B. J., Ransom, S. M., Freire, P. C. C., et al. 2017, *ApJ*, 845, 148, doi: [10.3847/1538-4357/aa7ed7](https://doi.org/10.3847/1538-4357/aa7ed7)
- Prochaska, J. X., & Zheng, Y. 2019, *MNRAS*, 485, 648, doi: [10.1093/mnras/stz261](https://doi.org/10.1093/mnras/stz261)
- Ransom, S. 2011, PRESTO: Pulsar Exploration and Search Toolkit. <http://ascl.net/1107.017>
- Ransom, S. M. 2001, PhD thesis, Harvard University
- Reich, P., & Reich, W. 1988, *A&A*, 196, 211
- Remazeilles, M., Dickinson, C., Banday, A. J., Bigot-Sazy, M. A., & Ghosh, T. 2015, *MNRAS*, 451, 4311, doi: [10.1093/mnras/stv1274](https://doi.org/10.1093/mnras/stv1274)
- Schlegel, D. J., Finkbeiner, D. P., & Davis, M. 1998, *ApJ*, 500, 525, doi: [10.1086/305772](https://doi.org/10.1086/305772)
- Schwab, J., Quataert, E., & Kasen, D. 2016, *MNRAS*, 463, 3461, doi: [10.1093/mnras/stw2249](https://doi.org/10.1093/mnras/stw2249)
- Shepherd, M. C., Pearson, T. J., & Taylor, G. B. 1994, in *Bulletin of the American Astronomical Society*, Vol. 26, 987–989
- Sieber, W., & Seiradakis, J. H. 1984, *A&A*, 130, 257
- Simha, V., Weinberg, D. H., Conroy, C., et al. 2014, arXiv e-prints, arXiv:1404.0402. <https://arxiv.org/abs/1404.0402>
- Sridhar, N., Metzger, B. D., Beniamini, P., et al. 2021, arXiv e-prints, arXiv:2102.06138. <https://arxiv.org/abs/2102.06138>
- Tendulkar, S. P., Gil de Paz, A., Kirichenko, A. Y., et al. 2021, *ApJL*, 908, L12, doi: [10.3847/2041-8213/abdb38](https://doi.org/10.3847/2041-8213/abdb38)
- Verbunt, F. 2003, in *Astronomical Society of the Pacific Conference Series*, Vol. 296, *New Horizons in Globular Cluster Astronomy*, ed. G. Piotto, G. Meylan, S. G. Djorgovski, & M. Riello, 245. <https://arxiv.org/abs/astro-ph/0210057>
- Wang, B., & Liu, D. 2020, *Research in Astronomy and Astrophysics*, 20, 135, doi: [10.1088/1674-4527/20/9/135](https://doi.org/10.1088/1674-4527/20/9/135)
- Webb, N., Cseh, D., Lenc, E., et al. 2012, *Science*, 337, 554, doi: [10.1126/science.1222779](https://doi.org/10.1126/science.1222779)
- Whitney, A., Kettenis, M., Phillips, C., & Sekido, M. 2010, in *Sixth International VLBI Service for Geodesy and Astronomy. Proceedings from the 2010 General Meeting*, ed. R. Navarro, S. Rogstad, C. E. Goodhart, E. Sigman, M. Soriano, D. Wang, L. A. White, & C. S. Jacobs, 192–196
- Yamasaki, S., & Totani, T. 2020, *ApJ*, 888, 105, doi: [10.3847/1538-4357/ab58c4](https://doi.org/10.3847/1538-4357/ab58c4)
- Yao, J. M., Manchester, R. N., & Wang, N. 2017, *ApJ*, 835, 29, doi: [10.3847/1538-4357/835/1/29](https://doi.org/10.3847/1538-4357/835/1/29)
- Ye, C. S., Fong, W.-f., Kremer, K., et al. 2020, *ApJL*, 888, L10, doi: [10.3847/2041-8213/ab5dc5](https://doi.org/10.3847/2041-8213/ab5dc5)
- Ye, C. S., Kremer, K., Chatterjee, S., Rodriguez, C. L., & Rasio, F. A. 2019, *ApJ*, 877, 122, doi: [10.3847/1538-4357/ab1b21](https://doi.org/10.3847/1538-4357/ab1b21)
- Yun, M. S. 1999, in *Galaxy Interactions at Low and High Redshift*, ed. J. E. Barnes & D. B. Sanders, Vol. 186, 81
- Zhong, S.-Q., & Dai, Z.-G. 2020, *ApJ*, 893, 9, doi: [10.3847/1538-4357/ab7bdf](https://doi.org/10.3847/1538-4357/ab7bdf)
- Zhou, P., Zhou, X., Chen, Y., et al. 2020, *ApJ*, 905, 99, doi: [10.3847/1538-4357/abc34a](https://doi.org/10.3847/1538-4357/abc34a)

## APPENDIX

## A. MODELLING OF [PR95] 30244 USING PROSPECTOR

We used the `Prospector` Bayesian inference code (Leja et al. 2017; Johnson et al. 2019) to estimate main physical properties of [PR95] 30244. Using the SDSS photometry (see Table 4; from the SDSS DR12 catalogue, Alam et al. 2015b)) and the Flexible Stellar Population Synthesis (FSPS) code (Conroy et al. 2009), it generated an underlying physical model of [PR95] 30244. To model the stellar population, it uses the MIST stellar evolutionary tracks and isochrones (Choi et al. 2016) based on MESA, an open-source stellar evolution package (Paxton et al. 2015). In this analysis, we used a parametric ‘delayed-tau’ star formation history (SFH) model with five free-parameters, which are described in Table 5. As we are modelling a globular cluster, we did not include nebular line emission but only enabled a dust emission model by Draine & Li (2007) in our fitting.

With this framework, we first ran `Prospector` and fit the SED model using Levenberg-Marquardt  $\chi^2$  minimization routine (Levenberg 1944). The best-fitted SED model is shown in Figure 6. `Prospector` then sampled the posterior using an Affine Invariant Markov chain Monte Carlo (MCMC) Ensemble sampler, `emcee` (Foreman-Mackey et al. 2013), and estimated uncertainties in the best fitted values of various physical properties of [PR95] 30244 that are stated in Table 3.

**Table 4.** Broadband SDSS filters used to model the SED of [PR95] 30244.

Instrument	Filter	Effective Wavelength [ $\text{\AA}$ ]	Flux density [maggie] <sup>a</sup>
SDSS	u	3546	2.92e-09
	g	4670	1.05e-08
	r	6156	1.77e-08
	i	7472	2.04e-08
	z	8917	2.33e-08

<sup>a</sup> The flux densities are assigned a 20% fractional uncertainty. Note that 1 maggie is defined as the flux density in Jansky divided by 3631.

**Table 5.** Free parameters and their associated priors for the `Prospector` ‘delayed tau’ model.

Parameter	Description	Prior
$\log(M/M_{\odot})$	total stellar mass formed	uniform: min=3, max=7
$\log(Z/Z_{\odot})$	stellar metallicity	top-hat: min=-3.5, max=0
dust2	diffuse V-band dust optical depth	top-hat: min=0.0, max=2.0
$t_{\text{age}}$	age of [PR95] 30244	top-hat: min=0.1, max=13.8
$\tau$	e-folding time of the SFH	uniform: min=0.1, max=30

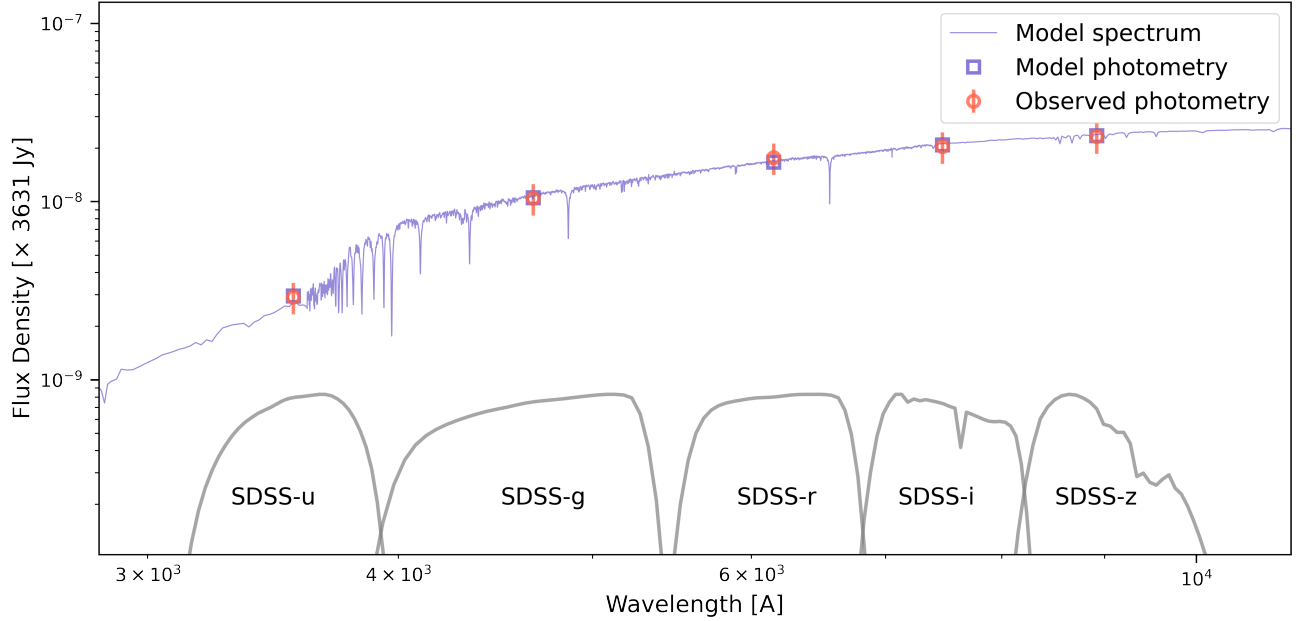


**Figure 6. Modelling the SED of [PR95] 30244.** The Milky Way extinction corrected flux density of [PR95] 30244 in different wavelength bands are plotted along with the best fitted Prospector model spectrum. To assess the quality of the Prospector model, the modelled and actual photometry data are also shown. The best fitted model profile is used to estimate different physical properties of [PR95] 30244 stated in Table 3.